

Role of electrostatic forces in cluster formation in a dry ionomer

Elshad Allahyarov

Department of Physics, Case Western Reserve University, Cleveland, Ohio 44106

and Joint Institute of High Temperatures,

Russian Academy of Sciences (IVTAN), Moscow, 125412 Russia

Philip L. Taylor

Department of Physics, Case Western Reserve University, Cleveland, Ohio 44106

Abstract

This simulation study investigates the dependence of the structure of dry Nafion[®]-like ionomers on the electrostatic interactions between the components of the molecules. In order to speed equilibration, a procedure was adopted which involved detaching the side chains from the backbone and cutting the backbone into segments, and then reassembling the macromolecule by means of a strong imposed attractive force between the cut ends of the backbone, and between the non-ionic ends of the side chains and the midpoints of the backbone segments. Parameters varied in this study include the dielectric constant, the free volume, side-chain length, and strength of head-group interactions. A series of coarse-grained mesoscale simulations shows the morphology to depend sensitively on the ratio of the strength of the dipole-dipole interactions between the side-chain acidic end groups to the strength of the other electrostatic components of the Hamiltonian. Examples of the two differing morphologies proposed by Gierke and by Gebel emerge from our simulations.

I. INTRODUCTION

Typical proton-conducting polymer electrolyte membranes (PEM) for fuel cell applications consist of a perfluorinated polymeric backbone and side chains that are terminated by strongly acidic sulfonic head groups. They provide the transport medium for the protons generated during the anodic oxidation reaction of the fuel. PEM fuel cells offer numerous advantages as power generators for emission-free vehicles, portable applications, and individual homes¹. When such ionomers are exposed to water or humid air, the acidic groups terminating the side chains dissociate into SO_3^- groups on the chains, and protons in the aqueous sub-phase. The sub-phase extends through the membrane, creating a bi-continuous nano-phase separated network of aqueous pores and polymer. The percolation structure and its ability to support proton diffusion have to meet strict requirements for a PEM to be considered as an ‘ideal’ membrane for fuel cells: a) It must form a chemically, mechanically, thermally and morphologically stable structure over a wide range of water content, b) show steady performance and tolerance of elevated temperatures up to 150°C at high proton conductance, and c) be impermeable to gases and contaminating ions. Development of new PEM membranes that could meet all these demands is a primary task for many research groups involved in fuel-cell studies.

One extensively used PEM material is Nafion[®], a perfluorinated polymer from DuPont. The integrity and structural stability of Nafion membranes is provided by the polytetrafluoroethylene (PTFE) backbones, but it is the hydrophilic clusters of side chain material that facilitate the transport of ions in the membrane. The microstructure of these clusters consists of an inter-facial region of solvated perfluoroether side chains separating the polymer matrix from the more bulk-like water found in the pores. In the presence of water, one finds a nano-separation of hydrophobic and hydrophilic domains. According to the early work of Gierke *et al.*^{2,3} these pores are inverted micellar spheres with diameters around 4 nm, and are interconnected by channels with a diameter and length of about 1 nm.

Recent experimental investigations suggest that the spherical shape and uniform spacing of these pores are serious oversimplifications⁴. New small-angle X-ray scattering (SAXS) and small-angle neutron scattering (SANS) experiments by Gebel *et al.*⁵ for Nafion membranes in different swelling states have given a different picture for the morphology. Their results suggest that elongated bundles of hydrophobic backbone material with diameters of about 4

nm and lengths greater than 100 nm are surrounded by sulfonate groups and water molecules. In other words, hydrophobic material is surrounded by hydrophilic domains.

The fact that controversy continues to surround the nature of the hydrated morphology and the shape of the domains suggests that there is still room for theoretical investigation and computer simulations to address this issue. *Ab initio* electronic structure calculations of polymeric fragments in contact with water⁶ and quantum molecular dynamics studies on model PEM systems⁷ have provided a basis for understanding the energetically favorable conformations of Nafion chains and the molecular ingredients of the conduction process^{8,9}. For systems large enough to contain several examples of hydrophilic inclusions and their interconnecting networks, however, treatment of the polymer in an *ab initio* manner, i.e. a full electronic treatment with molecular orbital theory, is not computationally feasible.

The objective of this paper is to develop a deeper understanding of the driving mechanism behind the nanophase aggregation of sulfonate head groups, and to test the extent to which coarse-graining methods can be applied. We attempt this by using a simple dipolar head group model for ionomer side chains. We show that the dipole-dipole correlations strongly depend on the molar fraction of acidic groups and dielectric permittivity of the membrane. Globular micelles formed in the case of zero dipole moment evolve to percolated cluster structures for a non-zero dipole moment of head groups when an artificial attraction between the end groups of side chains is introduced. Accounting for the dipole moment of sulfonate head groups thus changes the conformational structure of clusters from a Gierke model of spherical aggregations to a Gebel model of elongated aggregations. The determination of the parameters necessary for success in modeling nanophase aggregation will help us understand the essential role played by the electrostatic interactions of the head group in determining microstructure formation in PEM materials.

The rest of this paper is organized as follows. After a brief review of segregation models in section II, we present our dipolar model for side chains in section III. Section IV is devoted to our simulation results for dry PEM ionomers. We conclude with a discussion of results and planned future work in section V.

II. NANOPHASE SEGREGATION MODELS

Significant experimental and theoretical efforts have been put into the characterization of the microstructure of dry and swollen Nafion membranes. Although the fact of microphase segregation and its influence on the thermodynamic and transport properties of Nafion membranes are well established, some uncertainty regarding the morphology of the subphases in swollen Nafion remains. It has been generally assumed that the hydrophilic phase is continuous, in accord with the experimental evidence of high conductivity and water permeability. The conventional model of microphase segregation in Nafion membranes, put forward by Gierke *et al.*^{2,3}, where the protons and water diffuse between globular clusters through cylindrical narrow channels, was further modified by Mauritz and Rogers¹⁰ and Eikerling *et al.*¹¹. Also, Ioselevich *et al.*¹² developed a lattice based micelle-channel model to describe a connecting structure of a water bridges between the cages of the micelles. However, there is as yet no direct experimental evidence for the existence of the channels connecting the clusters in Gierke's model. Other models explaining the properties of hydrated Nafion exploit bilayer, lamellar, and sandwich-like structures for nanophase separation in PEM membranes. Gebel⁵ describes the Nafion membrane as an aggregation of polymeric chains forming elongated objects (simplified as cylinders), embedded in a continuous ionic medium. At larger scales, those aggregates form bundles with definite orientational order. This new picture of multi-scale structure can explain membrane swelling as a continuous process from the dry state to a colloidal suspension.

Scanning calorimetry experiments on cast Nafion films¹³ led to the conclusion that a continuous water phase exists only when the relative humidity of the membrane exceeds 90%. This conclusion contradicts the simulation results of Khalatur *et al.*¹⁴, where formation of continuous channels at very low hydration, and even in almost dry membranes, is reported. This is certainly consistent with the conductivity measurements in Nafion films with very little water present¹⁵. In contrast to all the above-mentioned network models, Vishnyakov *et al.*¹⁶ showed that the water clusters do not form a continuous hydrophilic subphase. Instead, the cluster-size distribution evolves in time as a consequence of the formation and rupture of temporary bridges between clusters.

Molecular dynamics (MD) studies, using both classical force fields and an *ab initio* approach, appear to support the idea of irregularly shaped ionic clusters of sulfonic groups

connected by smaller channels of similar composition embedded in the hydrophobic covalent matrix. However, the characteristic length scales of the morphological conformations suggested by experimental data are currently inaccessible to atomistic modeling. To probe the morphology at the nanometer scale, a mesoscale model is required.

III. DIPOLE MODEL FOR SIDE CHAINS.

In this work we are concentrating on the effects of electrostatic interactions among the elements of the side chains, and so in order to avoid the excessively slow processes resulting from chain entanglement we consider a segmented system in which the side chains are detached from the backbone. The later introduction of very strong interactions between the ends of the side chains and the backbone, which have the effect of knitting together the segments into a single macromolecule, do not seem to affect our results significantly.

A generic acidic side chain of Nafion is commonly denoted as $\text{CF}_3\text{OCF}_2\text{CF}(\text{CF}_3)\text{O}(\text{CF}_2)_2\text{SO}_3\text{H}$. In order to expedite these simulations, we adopt a simplified model for the side chain by using a united-atom presentation of the CF_2 and CF_3 groups^{16,17,18} and the SO_3^- sulfonate head groups¹⁹. These groups are modeled as Lennard-Jones (LJ) monomers. We employ the same united-atom approach for backbone chain segments.

In the framework of our dipole model all the partial charges on the ether oxygen, carbon and fluorine atoms of the side chain are set to zero. The fluorocarbon groups of the backbone skeleton are also assigned zero partial charges. The electrostatic charge is located entirely on the sulfonate head group, SO_3^- , and on the hydrogen ion H^+ permanently bound to it. The dipole moment produced when the proton and the sulfonate group, modeled as LJ monomers, carry the full formal charges of $+e$ and $-e$ respectively, was reduced by a factor D_r in some of our simulations. Though our model is not applicable for the measurement of proton diffusion in PEM membranes, it is a good starting point for a step-by-step exploration of the nanophase morphology in dry PEM materials.

The overall inter-monomer interaction in our model system is a combination of electrostatic Coulomb interactions between each pair of charged particles, 12-6 Lennard-Jones (LJ) potentials between neighboring monomers, and intrachain stretch and bend energies. The Lennard-Jones interaction parameters for the side chain are chosen to agree in most

instances with the Nafion model of Paddison²⁰. We make a further simplification for the LJ parameters of the side chain by assigning a universal value of σ , chosen to be 3.5 Å for all monomers. The total potential energy of the system is then given as

$$E_{\text{total}} = E_{LJ} + E_Q + E_{\text{bond}} + E_{\text{angle}}, \quad (1)$$

where E_{LJ} , E_Q , E_{bond} , and E_{angle} are the Lennard-Jones, electrostatic, bond-stretching (two-body term), and angle-bending (three-body term) components of the total energy, and are given by

$$E_{LJ}(r) = 4\epsilon_{LJ}(\sigma^{12}/r^{12} - \sigma^6/r^6) \quad (2)$$

$$E_Q = \sum_{i>j} \frac{Q_i Q_j e^2}{\epsilon R_{ij}} \quad (3)$$

$$E_{\text{bond}}(R) = \frac{1}{2} k_b (R - R_0)^2 \quad (4)$$

$$E_{\text{angle}}(\theta) = \frac{1}{2} k_\theta (\theta - \theta_0)^2 \quad (5)$$

We omit consideration of the dihedral potential term (four-body term), as this would be expected to make only a small contribution to the energetics of the single chain conformations in these dense polymeric systems. (This assumption was tested in sample simulations in which this term was restored, and found to have little effect on our results.) The following parameters for the polymer chains were used: an equilibrium bending angle $\theta_0 = 110^\circ$, an equilibrium bond length $R_0 = 1.54\text{Å}$ (0.44σ), a bending force constant $k_\theta = 120 \text{ kcal/mol deg}^2$, and a stretching force constant $k_b = 700 \text{ kcal/mol Å}^2$. The last two constants correspond to the thermal energy $k_B T$ at room temperature for a bond-length displacement of 0.1 Å and bond-angle displacement of 1° from the equilibrium position. The bond length between the SO_3^- head-group monomer and the hydrogen ion was chosen to be σ , and hence 0.35 nm. The LJ interaction coefficient ϵ_{LJ} was chosen to be $3k_B T$ for hydrophobic-hydrophobic (HH) interactions, and $1k_B T$ for both hydrophobic-hydrophilic (HP) and hydrophilic-hydrophilic (PP) interactions. In the latter case The LJ potential was modified to be purely repulsive by truncating at its minimum, where $r = 1.1224\sigma$, and raising it by the addition of an amount ϵ_{LJ} . The reason for this choice is that the interaction between protons is not well represented by van der Waals forces, which arise from virtual dipole-dipole interactions, and also that such attractive forces are small in comparison to the Coulomb interaction. The normalized charge Q_l ($l = i, j$) in Eq.(3) is +1 for protons and -1 for sulfonate groups.

We used this coarse-grained model to perform molecular dynamics simulations of ensembles of ionomer segments. Because chain entanglement greatly slows the rate of equilibration in polymers, we adopted the strategy of temporarily cutting the system into more mobile segments, which were later reassembled. In order to increase the diffusional rate of our model ionomer we detached the side chains from the backbone skeleton, an approach previously adopted by Vishnyakov²¹, and also cut the backbone skeleton into segments²². In total the system then consists of N_s sidechain segments and N_b backbone segments. Taking into account that the sulfonic acid groups are hydrophilic while the ethers and fluorocarbon groups are hydrophobic²⁰, we adopted the following general representation for a coarse-grained architecture of side chains and backbone segments. Each side chain contains $N_m = N_P + N_H$ monomers of which N_P are hydrophilic and N_H are hydrophobic. Its architecture is written as: $N_H\text{H}+N_P\text{P}$. The backbone segments are fully hydrophobic with an architecture $n\text{H}$. In the majority of systems studied in this paper, the side chain architecture was $8\text{H}+2\text{P}$ and the backbone segment architecture was 10H .

The simulations were then performed in several stages. The initial configuration was first prepared by using Monte-Carlo techniques to grow a mixture of polymer chain segments with fixed bending angle θ_0 and bond length R_0 . After an initial equilibration the constraints on θ_0 and R_0 were removed. Subsequently, MD runs were performed for time periods between 50ps and 500ps at constant volume V and constant temperature T until the system of polymer segments was fully equilibrated. The system temperature was controlled by coupling the system to a Langevin thermostat with a friction coefficient $\gamma = 0.1$ and Gaussian white-noise force of strength $6k_B T \gamma$. The equations of motion were integrated using the velocity Verlet algorithm with a time step of 0.5 fs. We imposed standard periodic boundary conditions to our system, filling space with translational replications of a fundamental cell. Long-range electrostatic interactions were calculated using the standard Lekner summation algorithm²³.

To check whether equilibrium had been reached we examined the proton pair distribution function $g(r)$ in every picosecond time interval, and continued the run until no significant further change was observed. To avoid mistaking the trapping of the simulated system into a metastable glassy state for true equilibrium, we repeated each run with several different initial configurations. For each computer experiment we typically gathered system statistics over time intervals of a few nanoseconds. We believe this to be sufficient to allow for the self-organization of the side chains and backbones into clustered structures.

In the next stage of the simulations the segments were reassembled into the branched chain characterizing the original Nafion. This was achieved by the simultaneous introduction of a specific mutually attractive force between the ends of each backbone segment, which united them into a single chain, and a similar force acting between the tail monomer of the detached side chains and the fifth monomer of every backbone segment. This was applied in the form of a LJ potential of strength $\varepsilon_{LJ} = 6k_B T$. To avoid the formation of star-like branched polymers, only a single occupancy of the backbone attachment sites was permitted. The simulation was then resumed, and run until a new equilibrium was attained. It was found that the bonds on the ends of all the backbone segments were occupied, and that a large majority (typically around 95%) of the side chains were reattached to a backbone segment. This fraction was a function of the ratio ψ of the number N_s of side chains (and hence of sulfonate groups) to the number $n \times N_b$ of backbone monomers. The quantity ψ thus measures the concentration of sulfonate groups relative to the concentration of backbone monomers. The few side-chains that did not bond to the special sites on the backbone attached themselves more loosely to the backbone through the weaker regular hydrophobic-hydrophobic LJ interaction potential.

We also introduce the absolute molar concentration of sulfonate groups, $\eta \equiv N_s/N_0 V_{\text{cell}}$, with N_0 being Avogadro's number and V_{cell} the volume L^3 of the simulation cell, as an alternative parameter with which to describe the sulfonate concentration, independently of the amount of backbone polymer. While it is true that in real dry Nafion, no significant free volume exists, and so the total number of monomers per unit volume is roughly fixed at the time of synthesis, in a simulation, however, it is possible to change the density of the material. It is of interest in understanding the mobility of ions in Nafion to know what structures would form in the presence of imposed free volume, were such a reduction in density of the material possible.

In order to observe the effects of the dipolar nature of the sulfonate-proton group on the structural characteristics of side chain aggregates, we calculated the normalized pair distribution function $g(r)$ of head group protons (which are the end group monomers of the side chains). The function $g(r)$ indicates the relative probability of finding two protons at a separation distance r averaged over the equilibrium trajectory of the simulated system, so that

$$g(r) = (V_{\text{cell}}/N_+) \frac{dn_+(r)}{4\pi r^2 dr}. \quad (6)$$

Here dn_+ is the number of protons located in a shell of thickness dr at the distance r from a fixed proton, and N_+ is the total number of protons in the system of volume V_{cell} .

In addition to this spherically averaged quantity, it is also useful to note some indications of the local anisotropy in order to distinguish between the Gierke and Gebel models. To this end we also evaluated the partial structure factors

$$S(q_j) = \left\langle \left[\sum_{i=1}^{N_+} \cos q_j r_i \right]^2 + \left[\sum_{i=1}^{N_+} \sin q_j r_i \right]^2 \right\rangle.$$

Here j denotes the x , y and z components of the vector \mathbf{q} , with $q_j = 2\pi n_j/L$, and the sums can proceed over the entire sample or over smaller volumes.

IV. SIMULATION RESULTS

The goal of these extensive coarse-grained molecular-dynamics simulations was to investigate the relative importance of the various model parameters on the aggregation of the sulfonate (acidic) head groups. To achieve this we performed a series of simulation runs in which the key parameters were varied as summarized in Table II. These parameters included the absolute concentration and the relative concentrations of side chains and backbone polymer, as well as the strength of the electrostatic interactions. This last quantity is characterized by a Coulomb coupling parameter defined as $\Gamma = e^2/\epsilon k_B T \sigma \equiv \lambda_B/\sigma$. Here λ_B , which is known as the Bjerrum length, is about 56 nm for a dielectric constant $\epsilon = 1$ and $T = 300$ K. The coupling parameter Γ was varied between 2 and 160 by varying the system dielectric permeability ϵ between 80 and 1, with higher Γ representing stronger electrostatic correlations in the system. In a typical simulation, a few thousand side chains are confined in a cubic box whose side is of length $L = 30\sigma$, with $\sigma = 0.3$ nm being the monomer diameter.

Each simulation run was started from a randomly generated assembly of side chains and backbone segments within the system volume. However, in order to avoid packing problems, and to make this process effective for high monomer densities, a preliminary simulation of the same number of monomers was first performed in a larger box of side $L' > L$, and this was then followed by a gradual reduction of the system volume until the desired molar concentration was achieved.

Table I: List of key variables.

D_r	dipole moment reduction factor
θ_0	equilibrium bending angle for backbone and sidechain polymers
R_0	equilibrium bond length for backbone and sidechain polymers
k_θ	bending force constant
k_b	stretching force constant
k_B	Boltzmann constant
T	system temperature
σ	monomer diameter
ε_{LJ}	Lennard-Johns interaction parameter between monomers
Q_e	normalized charge of sulfanates and ptorons
ϵ	dielectric constant of medium
N_s	number of side chains
N_b	number of backbone chain segments
N_m	number of monomers per side chain
N_H	number of hydrophobic monomers per side chain
N_P	number of hydrophilic monomers per side chain
n_b	number of hydrophobic monomers per backbone chain segments
ψ	ratio of the number of sulfonate groups to the number of backbone monomers.
η	molar concentration of head groups
N_0	Avogadro's number
L	length of simulation box
$g(r)$	proton-proton pair distribution function
n_+	local number of protons
N_+	number of protons in the system
V_{cell}	volume of simulation box
$S(q_j), j = x, y, z$	partial structure factors
Γ	coupling parameter in ionomer
λ_B	Bjerrum length

Table II: Parameters used in combinations for simulation runs. Here η is the molar sulfonate-ion concentration, N_b the number of backbone chain segments, L/σ the simulation cell size in units of $\sigma = 0.35$ nm, N_m is the number of monomers per sidechain, ψ is ratio of the number of sulfonate groups to the number of backbone monomers, and ϵ is the dielectric constant of the medium.

Runs	$\eta(\text{mol/l})$	N_b	L/σ	N_m	$n_b\psi$	ϵ	D_r
Run 1	0.8	0	30	10	0	1, 15, 80	1
Run 2	0.8	500	30	10	1	1, 15, 80	1
Run 3	0.8	1000	30	10	2	1	1
Run 4	0.8	1500	30	10	3	1	1
Run 5	0.8	2000	30	10	4	1	1
Run 6	0.8	2500	30	10	5	1	1
Run 7	1.6	0	30	10	0	1, 15, 80	0, 0.5, 1
Run 8	1.6	1000	30	10	1	1	0, 0.25, 0.5, 1
Run 9	1.6	2000	30	10	2	1	0, 0.5, 1
Run 10	0.2	1000	60	10	1	1	1
Run 11	0.5	1000	45	10	1	1	1
Run 12	2.5	1000	25	10	1	1	1
Run 13	0.16–4.8	0	30	10	0	1	1
Run 14	1.6	0	30	2–10	0	1	1

A. The role of the strength of the electrostatic interactions

In this first simulation the constraints imposed by the attachment of the side chains to the backbone were removed in order to concentrate on the effects of the electrostatic interactions. We then analyzed the proton-proton pair distribution function $g(r)$ calculated for an assembly of unattached side chains for three different dielectric constants ϵ of the ionomer medium, and for two different molar concentrations. The higher concentration, for which $\eta = 1.6$ mol/l, is characteristic of typical dry Nafion samples. Figure 1 shows the proton-proton pair distribution function for the parameters described in Table II as Run 1 and Run 7. The first observation is that, as expected, small ϵ , or, equivalently, high Γ ,

facilitates clustering of the head groups, as shown in the red dot-dashed lines in Figure 1. The graph of $g(r)$ shows well-defined maxima at $r/\sigma = 1.5, 2.0,$ and 3.4 . A detailed investigation shows that this is a consequence of the formation of three simple multiplet structures: compact and linear multiplets, each created by two head groups, and a branched multiplet composed of three head groups, as shown in Fig. 2.

For $\epsilon = 80$ there is no correlation between head groups on different side chains except for steric hindrances, as seen in the continuous blue lines in Figure 1. A more surprising result is the effective repulsion between acidic head groups at intermediate dielectric permittivities, as seen in the green dashed lines in Fig. 1. It appears that, in the absence of strong correlations, each head-group dipole prefers to stay in the bulk of the sample in order to increase its polarization energy. This is similar to the well known salt-depletion effect in colloidal physics, when salt pairs are effectively repelled from the surface of a neutral colloid²⁴.

The other unexpected result is the suppression of the correlations between the end groups at high molar sulfonate concentrations η , as seen in the dot-dashed line and symbols in Figure 1(b). This can be traced back either to the reduction of the Debye screening length, which effectively shields the dipoles from each other, or to the enhancement of the hydrophobic-hydrophobic attraction in the system. The latter emerges from the hydrophobic tails of the side chain segments.

To decide which of these two possible mechanisms was responsible, we added into the system described in Fig. 1(b) a small number of backbone segments in order to boost the effective hydrophobicity (or association energy) in our model system. One backbone segment of 10 monomers was added for each side chain unit, making $\psi = 0.1$. After equilibration, the side chains were then loosely attached to the backbone segments and the backbone segments were mostly united in the manner previously described, whereupon the system was further equilibrated. The results, shown as Run 2 in Figure 3, clearly indicate that the backbone segments have a minor impact on the head group distribution function. The system has almost the same microphase structure as observed for the original side chain system. A fivefold increase in the backbone concentration in Figure 3(b) has only a small effect on $g(r)$. Therefore, it is the dipole-dipole interaction that tends to destroy the correlations when the molar fraction of sulfonates is high. This effect takes place when the screening length becomes less than the mean separation distance between the dipoles. This has some

relevance to the search for ionomer membranes with superior transport properties: whereas for better proton conductance one needs a higher sulfonate molar fraction, the latter hinders sulfonate aggregation, which is vital for water-sulfur channel formation in wet ionomers.

Typical snapshots of the simulation box, shown in Figure 4, make visible the process of microphase separation in ionomer systems. The tips of the side chains, which correspond to end group protons, are shown as balls, whereas the rest of the side chains are plotted as lines. The backbone segments, drawn also as lines, mostly cluster together to create large aggregates. The side chains either anchor onto the surface of the backbone aggregate, or create their own small clusters.

Figure 5 presents a 3-dimensional density distribution of monomers for Run 5. The areas of low (high) density colored in blue (red) show the channel structure of the aggregates. The polymer matrix is composed of hydrophobic tails of side chains and backbone segments. The hydrophilic head groups form the walls of these channels. Though this 3D density picture differs from the long-bundle structural model of Nafion⁵, it supports the model of a dynamic system of non-spherical clusters with temporary inter-cluster bridges¹⁶.

B. Structure dependence on sulfonate molar concentration η .

In the previous section, in which we varied the strength of the Coulomb interactions, we observed that in the systems with the higher sulfonate concentration, the Coulomb correlations were suppressed. This suggested that a study of the morphology of aggregates over a wider range of concentrations would be helpful to understand the physics behind sulfonate cluster formation. Simulation results for $g(r)$ for systems with sulfonate concentrations η varying between 1.6 and 2.5 mol/l are shown in Fig. 6 for Runs 8 and 10-12. Results for the much wider range of 0.16 to 4.8 mol/l are shown in Fig. 7, but for these it was necessary to delete the backbone segments entirely in order to accommodate the very large concentration of side chains at the upper part of the range constituting Run 13.

The dipole-dipole correlations are seen to depend strongly on the molar concentration of acidic groups. For a typical dilute case, Run 10 in Fig. 6, the first peak of $g(r)$ reaches a value $g(r = 1.5\sigma) = 37$, indicating a strong condensation of nearly all the side chains. A possible explanation for this effect can be drawn from the clustering features of pure dipolar liquids. In a dilute system, where the average interchain distance is larger than the gyration radius R_g

of the side chain, the LJ interaction between the neighboring chains is negligible. The main contribution to the energy in this case comes from the electrostatic dipole-dipole interaction of head groups. Although this interaction decays with a $1/r^3$ distance dependence, it is not weak over distances comparable with the simulation box length L , and is capable of forcing the chains to aggregate. However, for a dense system, where the LJ contribution to the energy becomes comparable to the dipolar term, the side chains start to lose their rotational entropy, and thus cannot reorient themselves in order to minimize the electrostatic energy of the aggregate. While the heights of the maxima of $g(r)$ gradually decrease as the system becomes more tightly packed, their positions do not change and remain fixed at $r = 1.5\sigma$, 2σ , and 3.4σ .

The line with circles in Fig. 7 corresponds to the case where the concentration of backbone segments was double the case for Run 8, and corresponds to Run 9. It is seen that the proton pair distribution function is hardly affected by the existence of the extra hydrophobic segments. However this conclusion is not necessarily true for a system with the more attractive LJ parameters for HH and HP interactions that will be considered in section D. Both the snapshot picture in Fig. 8 and the 3D monomer density in Fig. 9 show microphase separation.

Another way to examine the head group clustering is to calculate the partial structure factors $S(q_j)$ ($j = x, y, z$) of the protons. Because these did not exhibit any marked anisotropy, an averaged $S(q)$ is plotted in Fig. 10. The position of the peak at $q\sigma = 4.2$ is associated with a correlation distance, $d = 1.5\sigma$ in the sample structure via the Bragg relationship $d = 2\pi/q$. A sharp growth at small q of the values of $S(q)$ in Fig. 10 results from microscopic aggregation of hydrophilic and hydrophobic monomers in the system.

To summarize the tendencies of dipole-dipole correlations presented in this and the previous section, we conclude that the hydrophilic head group aggregation takes place preferentially at low dielectric permittivity ϵ and low densities of sulfonate groups.

C. Role of side chain size N_M .

Although the bulk of this work describes the conformational structures of side chains of length $N_m=10$, it is worth while investigating systems with shorter side chains, since recent experiments²⁵ show a high proton transfer rate in ionomer membranes with shorter pendant

segments.

This section contains simulation results for different side chain lengths, $N_m = N_P + N_H$. The length of the hydrophilic part (the number of hydrophilic monomers) is fixed at $N_P = 2$ and the length of the hydrophobic tail (the number of hydrophobic monomers) N_H is varied between 0 and 8 (which corresponds to the variation of total side chain length N_m between 2 and 10) in order to reveal how the side chains' hydrophobic tail affects the pair distribution function of protons. No backbone material was included in these systems. Simulation results for Run 14 are shown in Fig. 11. Note that the case $N_m = 2$ corresponds to a system of dipolar dumbbells. Even a short hydrophobic tail with $N_m = 4$ strongly suppresses the aggregation of head groups. Thus the hydrophobicity of side chains, or the length of hydrophobic tail, is a strong obstacle to head group clustering. In other words, the dipole-dipole attraction between sulfonates of longer side chains is not sufficient to produce a nanophase separation. This conclusion is in contrast to the suggestion of Eisenberg²⁶ that each ionic group in the vicinity of a cluster of sulfonate groups is drawn in by dipolar attraction to form a depleted zone free of charge.

D. Ionomer morphology for strong hydrophilic and hydrophobic interactions.

One intriguing question in fuel cell technology is how the morphology of nanophase separation in PEM membranes depends on the polymeric structure of Nafion. In other words, what is the optimal comb-like structure for the ionomer to be a good material for a fuel cell? Using our segmental model for Nafion we can mimic different comb-like Nafion molecular conformations by changing the parameter ψ , which denotes the ratio of the number of sulfonate groups to the number of backbone monomers. The impact of ψ on the distribution function $g(r)$ was shown to be negligible for $\varepsilon_{LJ} = 3k_B T$ for HH and $\varepsilon_{LJ} = 1k_B T$ for both HP and PP interactions in Fig. 3 for Runs 1-6. In order to explore more generally the effect of changing ψ , we exaggerate the hydrophilic and hydrophobic interactions by tripling the interaction constants ε_{LJ} . The Results for Runs 1-3 presented in Fig. 12 for $\varepsilon_{LJ} = 9k_B T$ for HH, and $\varepsilon_{LJ} = 3k_B T$ both for HP and PP interactions, now show that the addition of backbone chain segments brings more conformational disorder into the head group correlations. This is also evident from the system snapshots for Run 3 in Fig. 13 for the two different strengths of Lennard-Jones interaction parameters. In other words, a strong interaction

between hydrophobic and hydrophilic monomers can disrupt the side chain aggregation, causing all the side chains to be evenly distributed on the surface of backbone aggregations, as in Fig. 13(b). This distribution will have a globular, lamellar, or cylindrical-rod form.

E. End group attraction between side chains

To complete this study of the effects of interactions on morphology, we look at the effect of both decreasing and increasing the interaction between head groups. We have already seen in section IIIA some of the consequences of reducing the Coulomb interaction by increasing the dielectric constant ϵ . In the absence of interactions other than the dipole-dipole interaction, this is equivalent to a reduction in the strength of the dipole moments. In Fig. 14 we show the effect on the structure factor $S(q)$ of the protons of a reduction in the strength of the dipole moments by various factors D_r (Run 8). When the parameter D_r is small, there is no phase separation in the ionomers, and the function $S(q)$ has a liquid-like structure with a single maximum. The behavior of $S(q)$ is changed for an unreduced dipole strength $D_r=1$ in a manner similar to the behaviour of $S(q)$ in the less dense system shown in Fig. 10: there is a strong peak at $q\sigma=4.2$, and a sharp growth at small $q\sigma$. The latter, again, is an indication of a strong microscopic separation of hydrophilic and hydrophobic monomers in the system.

It is clear that the effective attraction between the acidic groups of side chains cannot be accounted for by the sulfonate-hydrogen dipole moment alone. The sulfonate end group has its own internal dipole moment due to the charge distribution between the sulfur atom and the three oxygen atoms bound to it. Partial charges on the other side chain monomers can also contribute to the effective attraction between head groups. To take all these contributions into account at a phenomenological level we introduce an artificial attractive interaction between the end groups of the side chains, in an approach similar to that employed by Shirvanyanz²⁷. For this purpose we use a Yukawa-type attractive potential,

$$F(r) = -(Z^2 e^2 / \epsilon r) \exp(-r/r_D) \text{ for } r > \sigma; \quad F(r) = \infty \text{ for } r < \sigma.$$

Here Z is an effective Yukawa charge for the head group sulfonates. For the sake of simplicity, we restrict ourselves to the case of constant Debye screening length $r_D = 4\sigma$. In fact, the parameters Z and r_D determine the stability, size and shape of the aggregates forming in the

system. The simple attractive Yukawa term can serve as a convenient basis for interpreting all the important features that can be observed in real systems or predicted by statistical mechanical theories.

In the absence of electrostatic interactions in the system, i.e. when the head group dipole moment vanishes and $D_r = 0$, the ionomer system becomes spatially inhomogeneous. The pair distribution functions $g(r)$ for Runs 7-9, plotted in Fig. 15 for $Z = 0.1$ (case (a)) and $Z = 0.5$ (case (b)) show strong structuring. The aggregation is substantially stronger for a system missing backbone polymer (Run 7) than for a system with a full complement of backbone monomers (Run 9), as seen from a comparison of the respective lines in Fig. 15. There is a clear tendency to micellar arrangement, which is characterized by some short-range order. Snapshot pictures, given in Fig. 16, show formation of a space-filling web-like network of cluster-like aggregates surrounded by neutral polymer sections. The size of these clusters grows as the density of side chains increases. A comparison of Figs. 16(a) and 16(b) reveals that the effective Yukawa charge Z , or in other words, the strength of the screened Coulomb attraction, has a strong impact on the shape of the clusters. The structure of the system for a moderate Yukawa attraction of $Z = 0.1$ between the end groups is mobile: the aggregates can diffuse, decay and reappear again. They can also create temporary bridge-like connections. Therefore the nanophase separation of the head groups, shown in Fig. 16(a) can be viewed as an example for a Gierke-like sulfonate aggregation. However, a strong attraction between the end groups of the side chains, the case $Z = 0.5$ in Fig. 16(b), results in a frozen network of globular clusters of diameter roughly 1.5 nm in the polymer matrix. This cluster picture resembles the ion segregation phenomenon proposed by Eisenberg²⁶.

When the dipole moment of the sulfonate head groups is restored, in this case with a value of $D_r = 0.5$, the globular micelles form super-clusters of diameter 3-4 nm, as seen in Fig. 17(b) for $Z = 0.5$. On the other hand, this nonzero dipole moment facilitates the formation of percolated cluster structures for $Z = 0.1$, as in Fig. 17(a). The inclusion of the dipole moment of the sulfonate head groups thus changes the conformational structure of clusters from a Gierke model of spherical aggregations to a Gebel model of elongated aggregations. A snapshot picture of the same system but with no artificial attraction between the head groups is given in the Fig. 18. It is clear that the introduction of a screened Coulomb attraction results in the formation of compact and interconnected clusters of sulfonate head groups.

V. CONCLUSIONS

In this study we have explored the issue of nanophase separation in dry Nafion[®] films by means of simulations within a simple dipolar-head-group model for the side chains. Our procedure involved detaching the side chains from the backbone and cutting the backbone into segments to speed equilibration, and then reassembling the macromolecule by means of a strong imposed attractive force between the cut ends of the backbone, and between the non-ionic ends of the side chains and the midpoints of the backbone segments.

As we vary the interaction parameters and dielectric permittivity of the medium we find different structures to be formed by the head groups. Small permittivities facilitate the clustering of head groups with a well defined maximum in the proton-proton pair distribution function $g(r)$ that indicates three simple multiplet structures: compact and linear multiplets each created by two head groups, and a branched cluster composed of three head groups. At higher permittivity no correlations between head groups are obtained. An effective repulsion between acidic head groups at intermediate dielectric permittivities was revealed from our data. We assume that, in the absence of strong correlations, each head-group dipole prefers to stay in the bulk of the sample in order to increase its polarization energy.

For the ionomer interaction parameters considered in this work the microphase structure of the head groups was found to have little dependence on the concentration of backbone segments. Since the molar fraction of sulfonates in a fuel cell membrane is known to be a crucial parameter for its performance, this factor was also studied. We find that for a dilute case a strong condensation of nearly all side chains takes place. The main contribution to the Hamiltonian in this case comes from a long-range dipole-dipole interaction of head groups which forces the chains to aggregate. However, for a dense system, where the hydrophobic LJ contribution to the Hamiltonian becomes comparable with the dipolar term, the side chains cannot reorient themselves in order to minimize the electrostatic energy of the aggregate. While on the one hand, for high proton conductance one needs higher sulfonate molar fractions η , on the other hand we find that a high value of this parameter η hinders the sulfonate aggregation that is vital for water-sulfonate channel formation in ionomers.

Overall, our simulations show that the dipole-dipole interaction is the main driving force for the aggregation of sulfonates. When the dipole moment of sulfonates is small, so that $D_r \ll 1$, there is no phase separation in the ionomers. In contrast, for $D_r = 1$ a microscopic

aggregation of hydrophilic and hydrophobic monomers takes place in the system.

The most significant feature learned from the simulations is the fact that the dipolar-head-group approximation is not sufficient to drive the compact side chain cluster formation suggested by experimental measurements. An additional artificial attraction between the sulfonates, introduced as a screened Yukawa interaction potential, boosts formation of nanometer-sized clusters dispersed throughout the system volume. The final size of these clusters, and the geometry of the cluster network they create, depend on the dipole moment D_r of the sulfonate head groups for fixed Yukawa parameters. As the strength of D_r increases from zero to one, the conformational structure of clusters changes from a Gierke model of spherical aggregations to a Gebel model of elongated aggregations.

More work is required to develop a deeper understanding of the mechanisms behind the aggregation picture observed experimentally. Because the shape and size distribution of the aqueous pores in wet membranes is not completely known, it will be useful to extend our preliminary results for the dry Nafion considered in this paper to systems with water present and with a more detailed chain structure. In future work, we plan to extend the model presented here to more complex models. In particular we will employ partial charges and Lennard-Jones parameters^{16,17,28} for side chain and backbone monomers of Nafion-like oligomers. The issues of how the partial charges of ionomer molecules, in fixed and free proton models for side chains, affect the nanophase structure of the PEM materials will be addressed. A complete understanding of the role of head group charges on the cluster conformations of side chains can provide helpful guidelines for understanding existing membranes and designing new membrane materials for fuel cells with improved characteristics.

Acknowledgments

This work was supported by the US Department of Energy under grant DE-FG02-05ER46244, and was made possible by use of facilities at the Case ITS High Performance Computing Cluster and the Ohio Supercomputing Center.

¹ M. I. Perry, T. F. Fuller, *J. Electrochemical Society* **149**, S59 (2002).

² T. D. Gierke, G. E. Munn, F. C. Wilson, *J. Polym. Sci. Phys. Ed.* **19**, 1687-1704 (1981).

- ³ W. Y. Hsu, T. D. Gierke, *Macromolecules* **15**, 101-105 (1982); *ibid* *J. Memb. Sci.* **13**, 307-326 (1982).
- ⁴ S. J. Paddison, *Annu. Rev. Mater. Res.* **33**, 289-319 (2003).
- ⁵ G. Gebel, O. Diat, *Fuel Cells* **5**, 261 (2005); I. Rubatat, O. Diat, G. Gebel, *Physical chemistry and Soft Matter* **106**, 1 (2004).
- ⁶ S. J. Paddison, J. A. Elliott, *J. Phys. Chem.* **109**, 7583 (2005).
- ⁷ M. Eikerling, S. J. Paddison, L. R. Pratt, T.A. Zawodzinski Jr., *Chem. Phys. Letters* **368**, 108 (2003).
- ⁸ K. D. Kreuer, S. J. Paddison, E. Spohr, M. Schuster, *Chem. Rev.* **104**, 4637 (2004).
- ⁹ T. Li, A. Wlaschin, P. B. Balbuena, *Ind. Eng. Chem. Res.* **40**, 4789-4800 (2001).
- ¹⁰ K. A. Mauritz, C. E. Rogers, *Macromolecules* **18**, 483 (1985)
- ¹¹ M. Eikerling, A. A. Kornyshev, U. Stimming, *J. Phys. Chem. B* **101**, 10807 (1997).
- ¹² A. S. Ioselevich, A. A. Kornyshev, J. H. G. Steinke, *J. Phys. Chem. B* **108**, 11953 (2004).
- ¹³ M. Laporta, M. Pegoraro, L. Zanderighi, *Phys. Chem. Chem. Phys.* **1**, 4619-4628 (1999).
- ¹⁴ P. G. Khalatur, S. K. Talitskikh, A. R. Khokhlov, *Macromol. Theor. Simul.* **11**, 566-586 (2002).
- ¹⁵ T. A. Zawodzinski Jr., M. Neeman, L. O. Sillerud, S. Gottesfeld, *J. Phys. Chem.* **95**, 6040-6044 (1991).
- ¹⁶ A. Vishnyakov, A. V. Neimark, *J. Phys. Chem. B* **105**, 7830 (2001); *ibid* 9586-9594 (2001).
- ¹⁷ J. T. Wescott, Y. Qi, L. Subramanian, T. W. Capehart, *J. Chem. Phys.* **124**, 134702 (2006).
- ¹⁸ S. Yamamoto, R. Jinnouchi, Sh. Yamakawa, Sh. Hyodo, 14th International Conference on the Properties of Water and Steam, Kyoto, Japan, p.411 (2004).
- ¹⁹ E. Spohr, *Molecular simulations* **30**, 107 (2004).
- ²⁰ S. J. Paddison, T. A. Zawodzinski, *Solid State Ionics* **113-115**, 333-340 (1998).
- ²¹ A. Vishnyakov, A. V. Neimark, *J Phys. Chem. B* **104**, 4471 (2000); D. Rivin, G. Meermeier, N. S. Schneider, A. Vishnyakov, and A. V. Neimark, *J. Phys. Chem. B* **108**, 8900 (2004).
- ²² S. C. Glotzer, W. Paul, *Annu. Rev. Mater. Res.* **32**, 401-436 (2002).
- ²³ M. Mazars, *J. Chem. Phys.* **115**, 2955-2965 (2001).
- ²⁴ E. Allahyarov, J.-P. Hansen, A. Lous, H. Löwen, *Europhys. Letters* (2005).
- ²⁵ V. Arcella, A. Ghielmi, G. Tommasi, *Ann. N. Y. Acad. Sci.* **984**, 226 (2003).
- ²⁶ A. Eisenberg, *Macromolecules* **30**, 7914 (1997).
- ²⁷ D. G. Shirvanyanz, A. S. Pavlov, P. G. Khalatur, *J. Chem. Phys.* **112**, 11069 (2000).

²⁸ S. S. Jang, V. Molinero, T. Cagin, W. A. Goddard III, *J. Phys. Chem. B* **108**, 3149-3157 (2004).

Figure 1: (Color online) Proton-proton pair distribution function $g(r)$ for (a) Run 1 (low density), and (b) Run 7 (high density) for $\epsilon=1$ (dot-dashed line), 15 (dashed line) and 80 (full line). Simulation results for $\epsilon=1$ are scaled down by a factor of four to fit the figure dimensions. The $\epsilon = 1(*)$ (symbols) in (b), given for comparison, corresponds to the $\epsilon = 1$ line in (a).

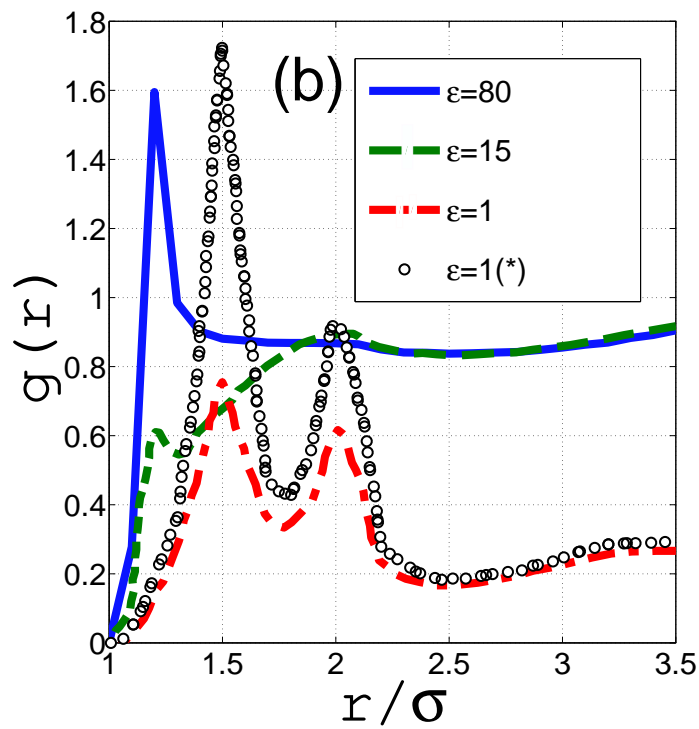
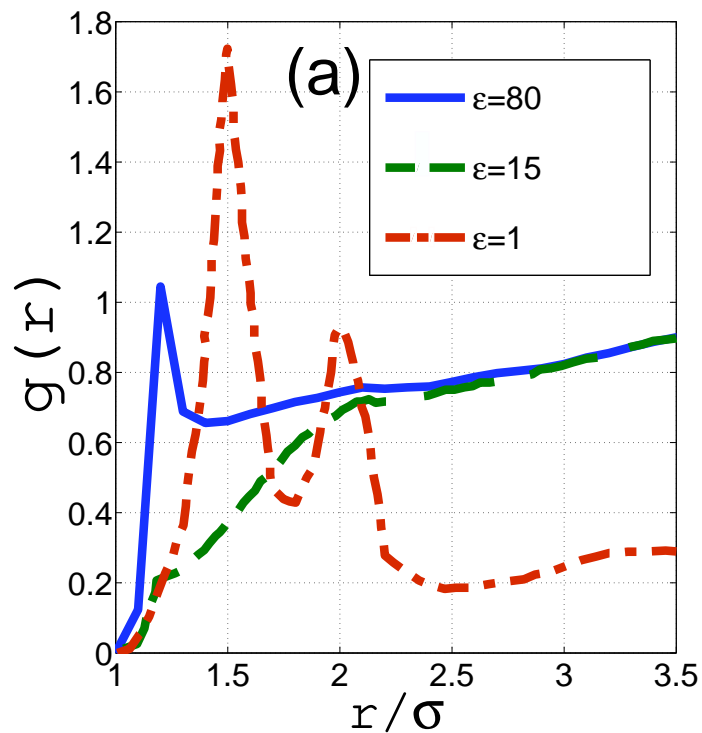


Figure 2: (Color online) Simple multiplet structures in side chain aggregates. Upper row: compact (left) and linear (right) multiplets. Bottom row: branched multiplet. The hydrophobic tails are shown only for a compact multiplet. The dashed objects C and D for the branched cluster indicate another possible configuration of objects A and B respectively. Positively charged hydrogen atoms are shown as yellow circles.

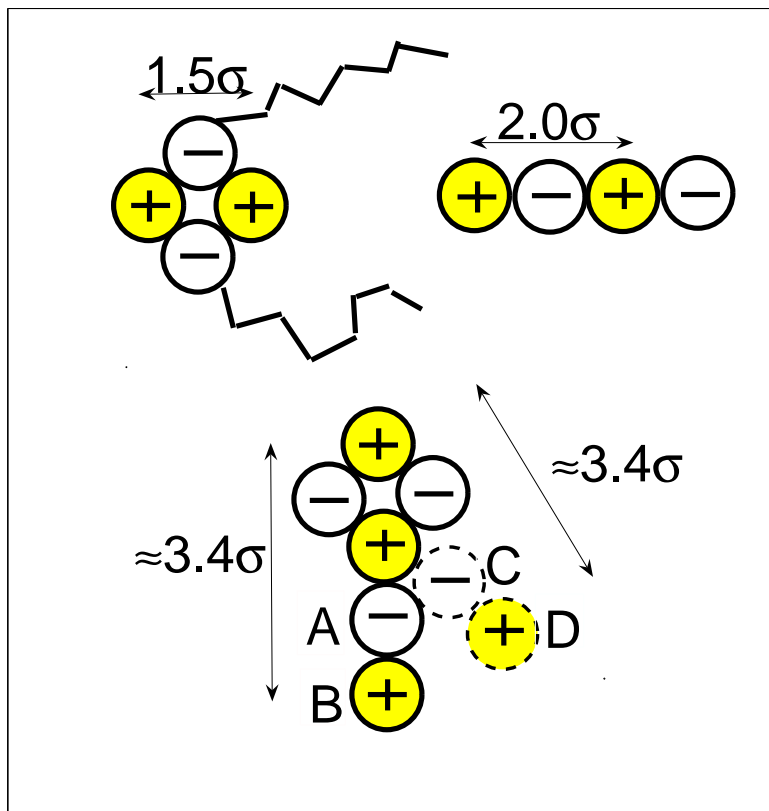


Figure 3: (Color online) (a) Proton-proton pair distribution function $g(r)$ for Run 2 and different dielectric permittivities. $\epsilon=1$ (dot-dashed line), 15 (dashed line) and 80 (full line). Results for Run 1, not shown here, are very close to the results for $\epsilon=1$. Simulation results for $\epsilon=1$ are scaled down by a factor of four to fit the figure dimensions. (b) Proton-proton pair distribution function $g(r)$ for different amounts of backbone polymer (Runs 2 and 6). Results for Run 3-5 (not shown here) that correspond to intermediate amount of backbone polymer, lay between these two curves.

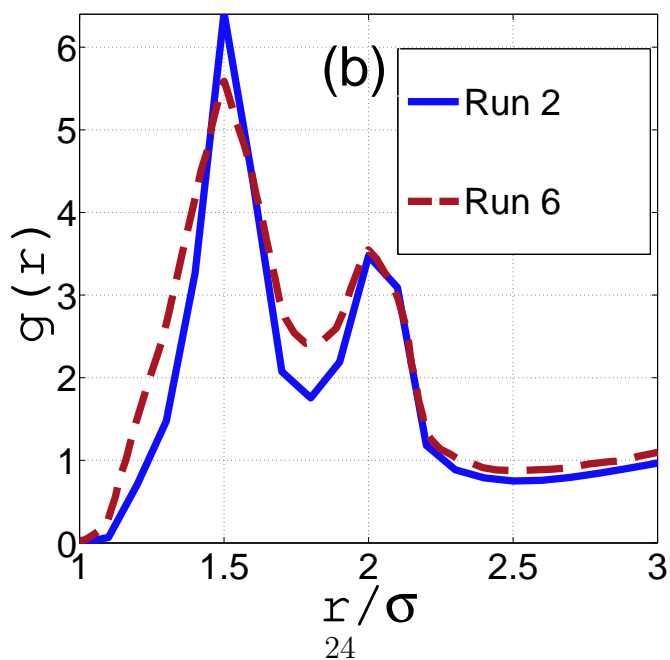
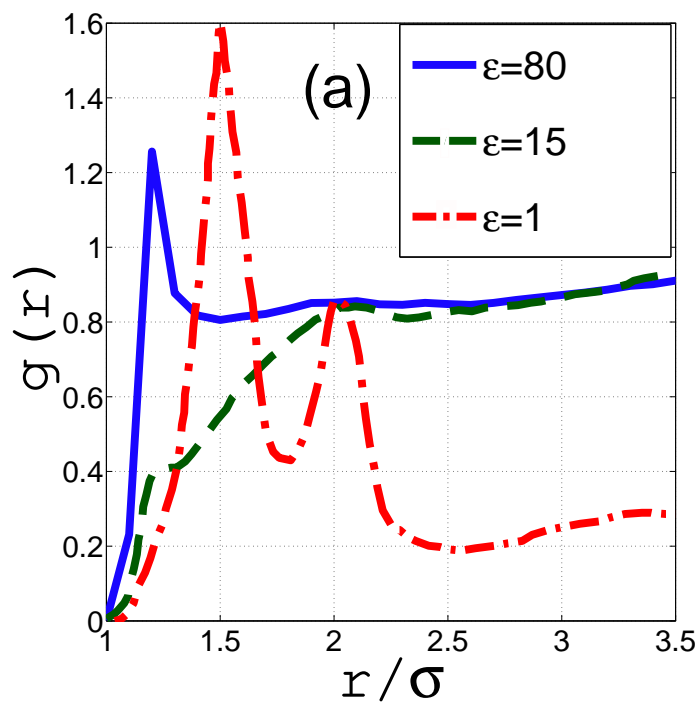


Figure 4: (Color online) Typical snapshots of a system for Run 4 (case (a)), and Run 6 (case (b)). Spheres represent the end-groups (protons) of side chains. The sulfonate group and neutral chain sections are drawn by lines (in red in online version). Different bead colors correspond to different bead altitudes, with a blue color for low-altitude beads (at the bottom of simulation box) and a red color for high-altitude beads (at the top of simulation box). The size of all the structural elements is schematic rather than space filling.

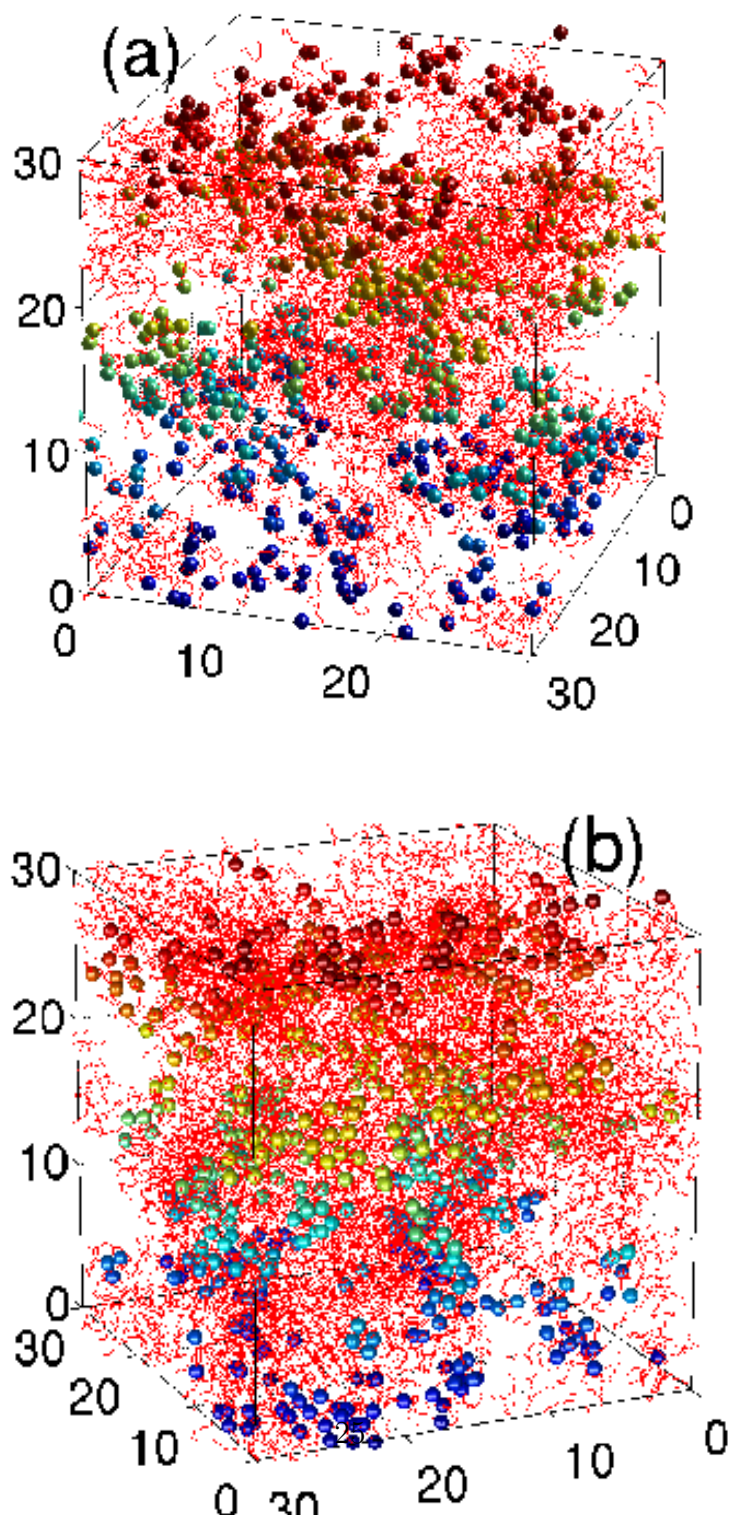


Figure 5: (Color online) A short-time average of the 3D density of monomers for Run 5. The hydrophobic tails of side chains and backbone segments create a solid matrix, whereas the hydrophilic head groups forms the walls of the channels.

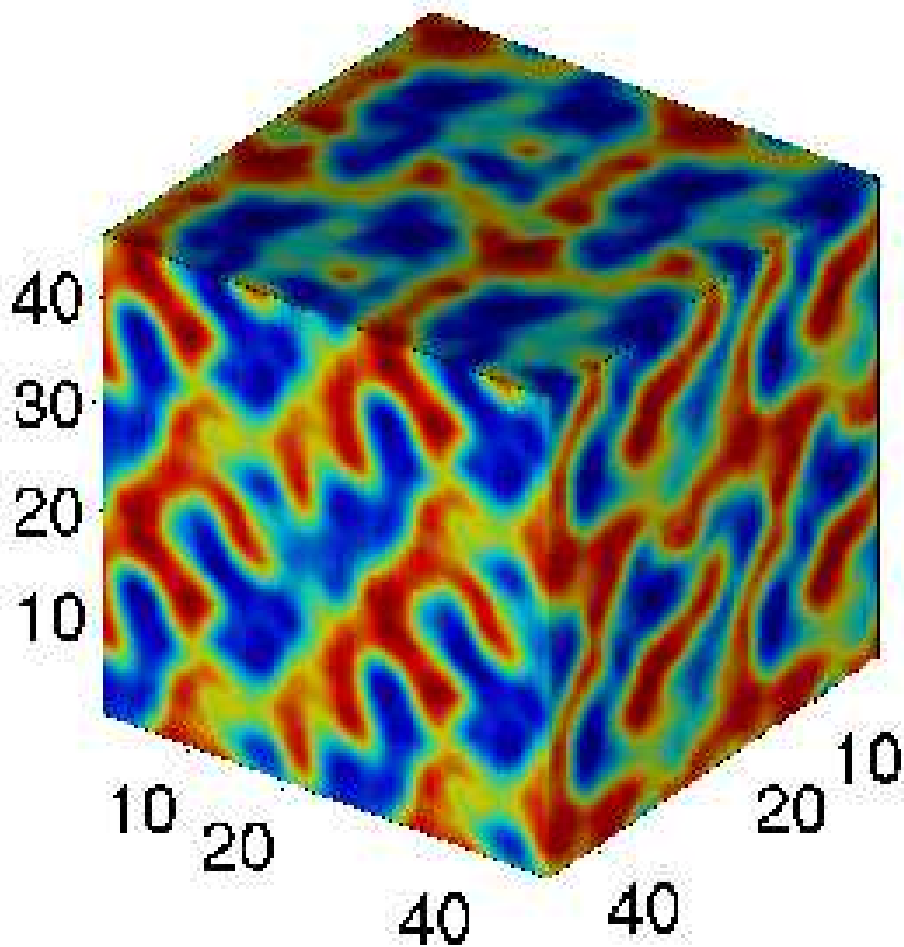


Figure 6: (Color online) Proton-proton pair distribution function $g(r)$ for different box sizes L , and hence sulfonate concentrations η , for Runs 8 and 10-12. The first peak of $g(r)$ for Run 10 (full line, blue in colored figure) has a value $g(r = 1.5\sigma) = 37$, out of the scale of the plot.

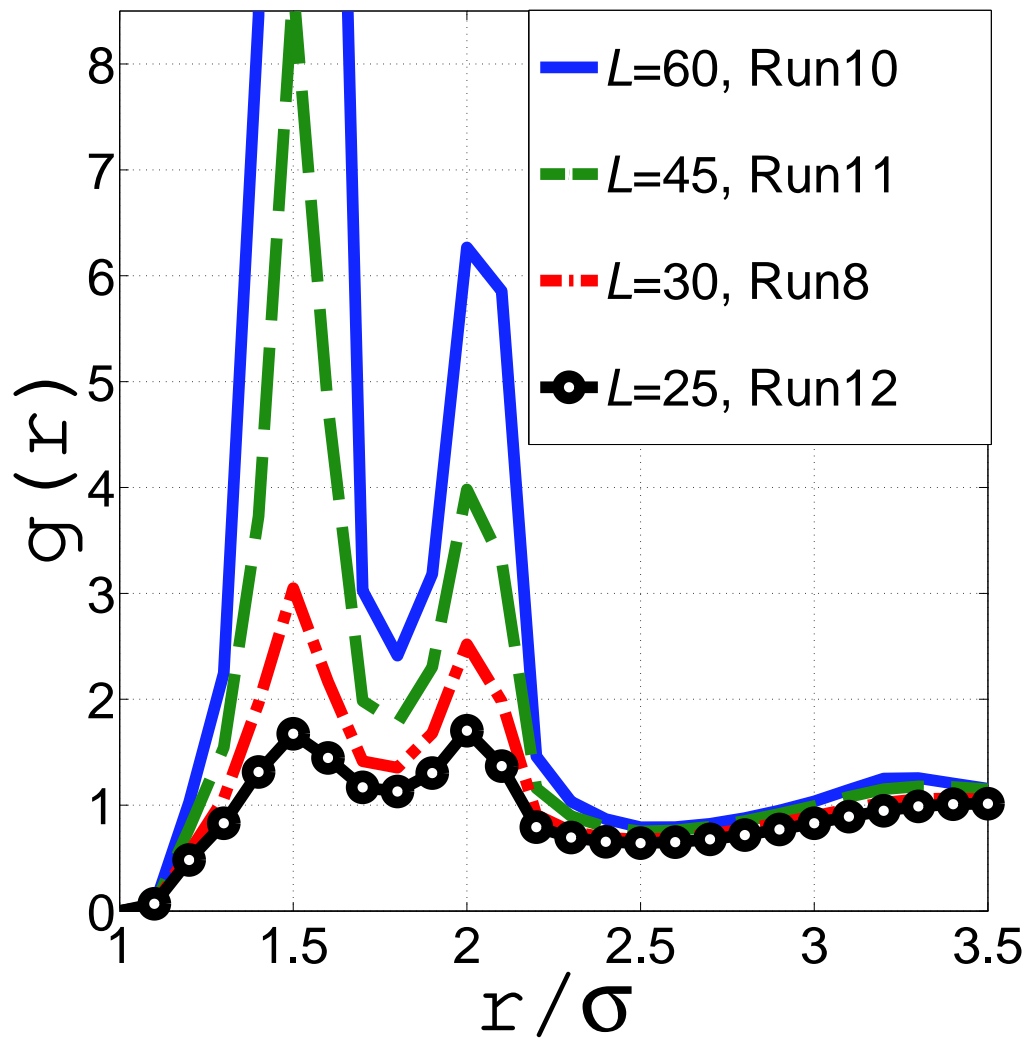


Figure 7: (Color online) Proton-proton pair distribution function $g(r)$ for different sulfonate molar concentrations η , Run 13. (a): $0.16 \text{ mol/l} \leq \eta \leq 1.6 \text{ mol/l}$. (b): $1.6 \text{ mol/l} \leq \eta \leq 4.8 \text{ mol/l}$. The case $\eta = 1.6(*)$ (line with circles in (b)) is for Run 9. The first peak of $g(r)$ for $\eta = 0.16$ ($\eta = 0.32$) mol/l (full blue line (dashed green line) in (a)) has a value $g(r = 1.5\sigma) = 53$ ($g(r = 1.5\sigma) = 22$), which is out of the scale of the plot.

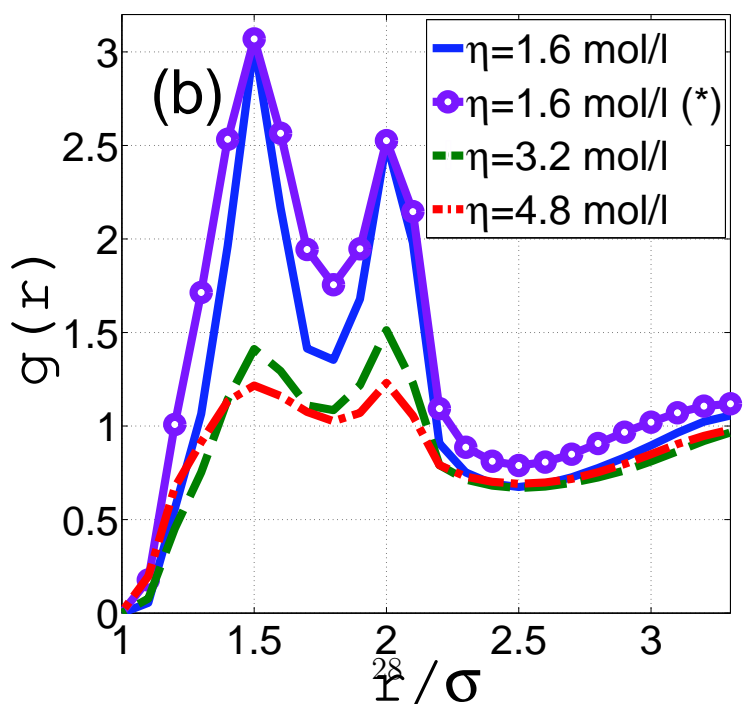
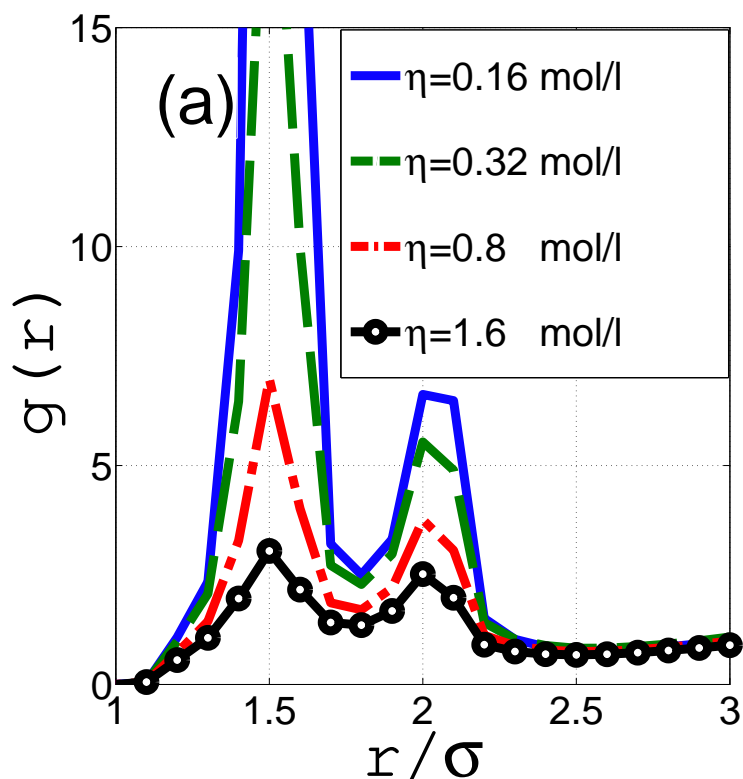


Figure 8: (Color online) Typical snapshots of system for Run 13 containing $\eta = 0.4\text{mol/l}$ (case (a)) and $\eta = 3.2\text{ mol/l}$ (case (b)) head groups.

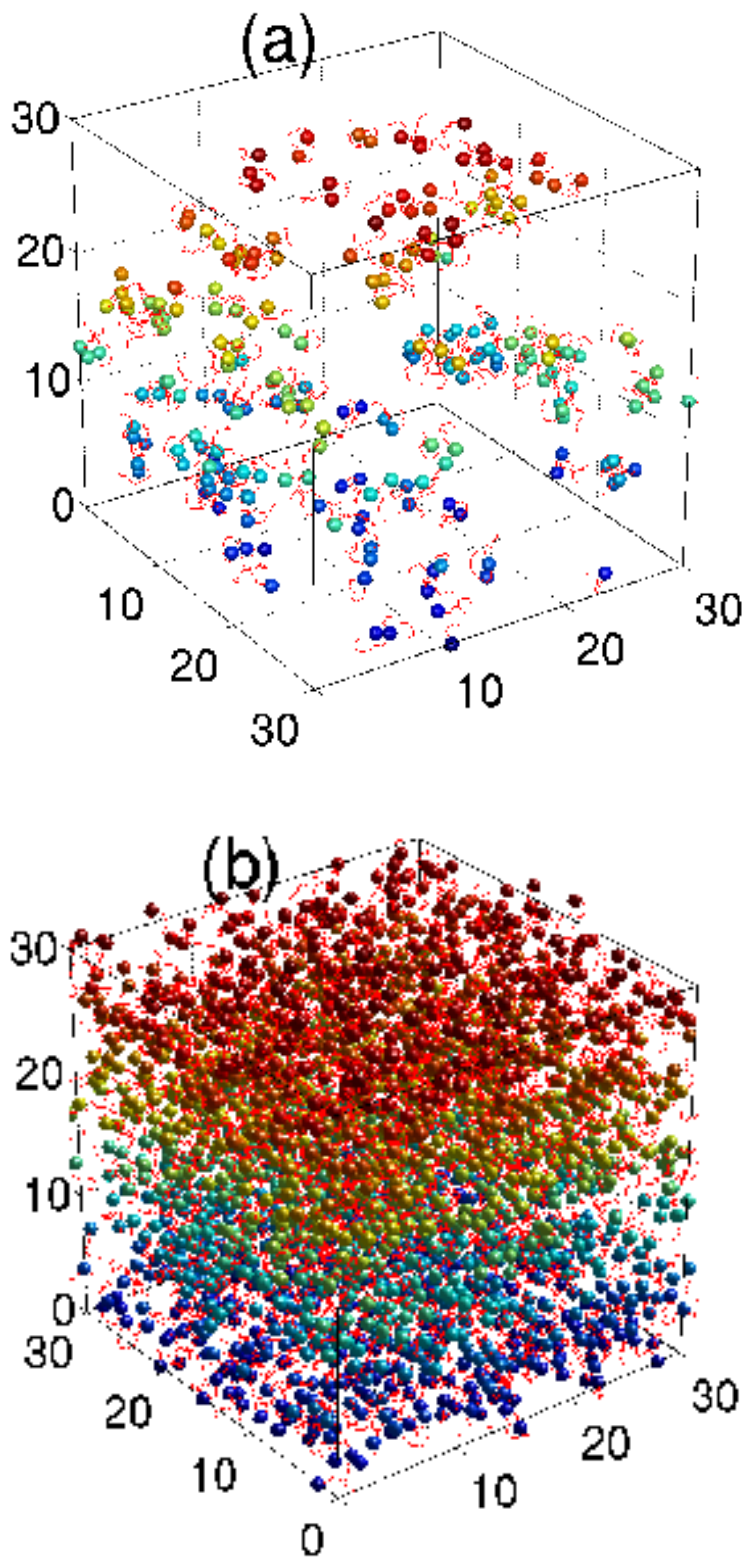


Figure 9: (Color online) A short-time average of 3D density of ionomer monomers for Run 13 and $\eta = 2.4$ mol/l. The areas of low density are cut away.

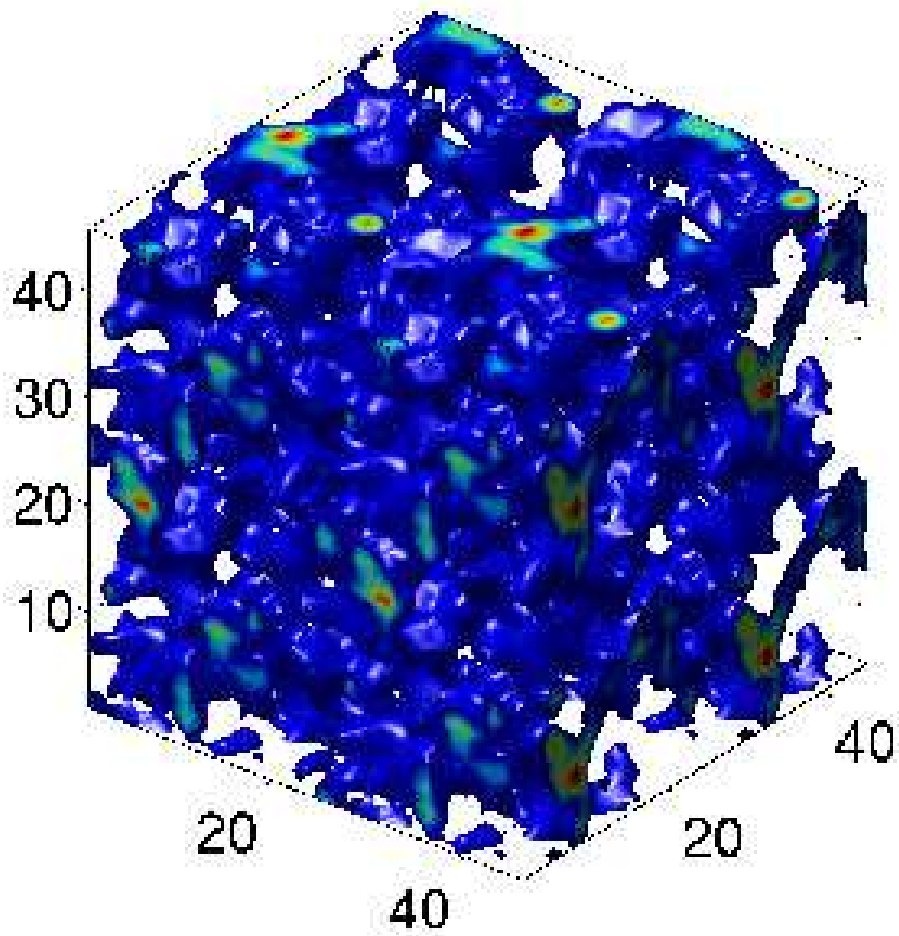


Figure 10: (Color online) Structure factor $S(q)$ of the head groups for Run 3 versus wave number $q\sigma$.

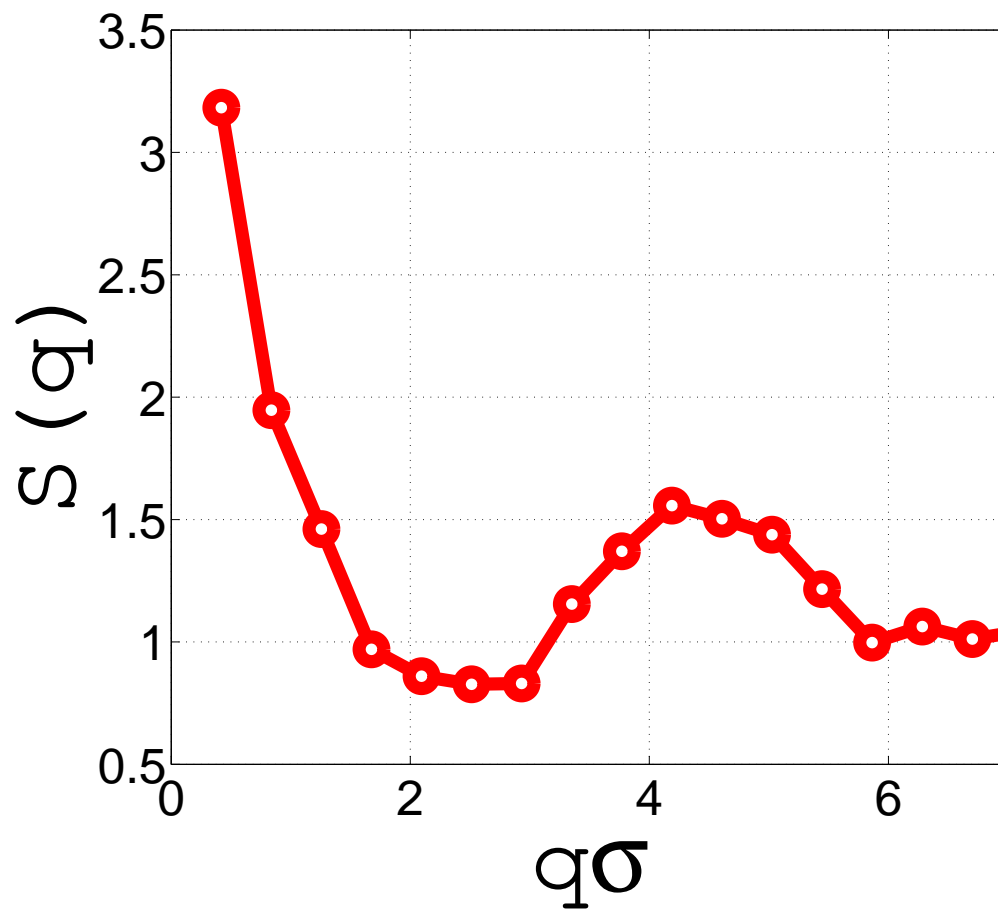


Figure 11: (Color online) Proton-proton pair distribution function $g(r)$ for a system of side chains for Run 14. The number of monomers per side chain segment N_m is changed from 2 to 10.

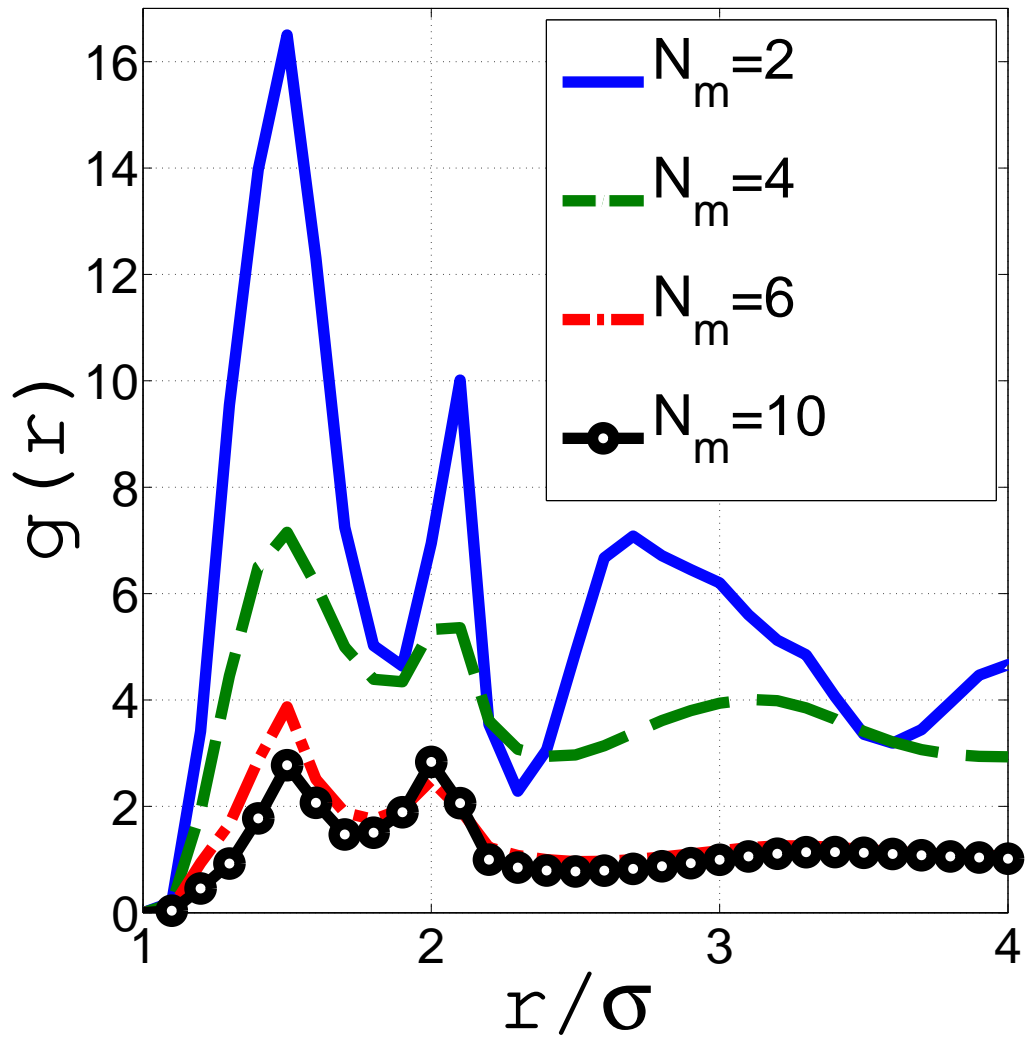


Figure 12: (Color online) Proton-proton pair distribution function $g(r)$ for Run 1 (solid line), Run 2 (dashed line) and Run 3 (dot-dashed line). Thick lines: $\varepsilon_{LJ} = 9k_B T$ for hydrophobic-hydrophobic (HH) interaction, $\varepsilon_{LJ} = 3k_B T$ for hydrophobic-hydrophilic (HP) and hydrophilic-hydrophilic (PP) interactions. Thin lines: $\varepsilon_{LJ} = 3k_B T$ for HH, $\varepsilon_{LJ} = 1k_B T$ for HP and PP interactions.

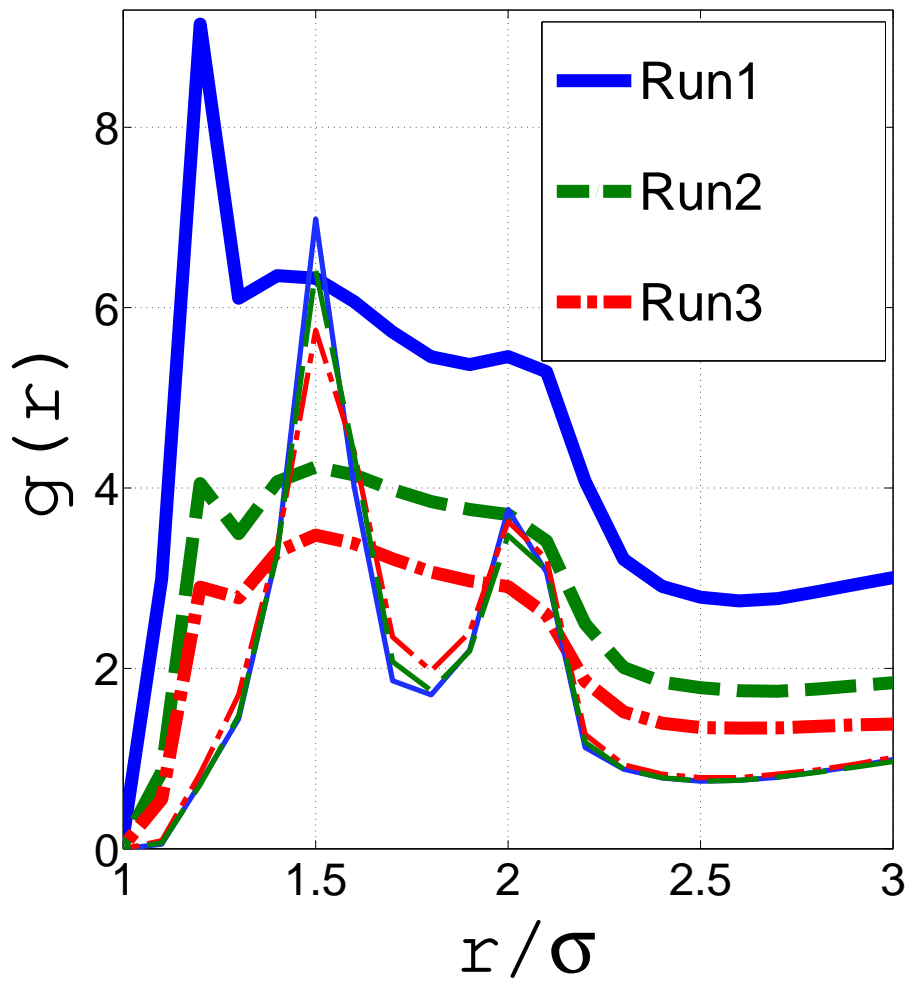


Figure 13: (Color online) Snapshot pictures of systems for Run 3 and $n_b\psi = 2$. Case (a): $\varepsilon_{LJ} = 3k_B T$ for HH, $\varepsilon_{LJ} = 1k_B T$ for HP and PP interactions. Case (b): $\varepsilon_{LJ} = 9k_B T$ for HH and $\varepsilon_{LJ} = 3k_B T$ for HP and PP interactions. In the case (b) the sulfonate groups are mostly on the surface of clusters.

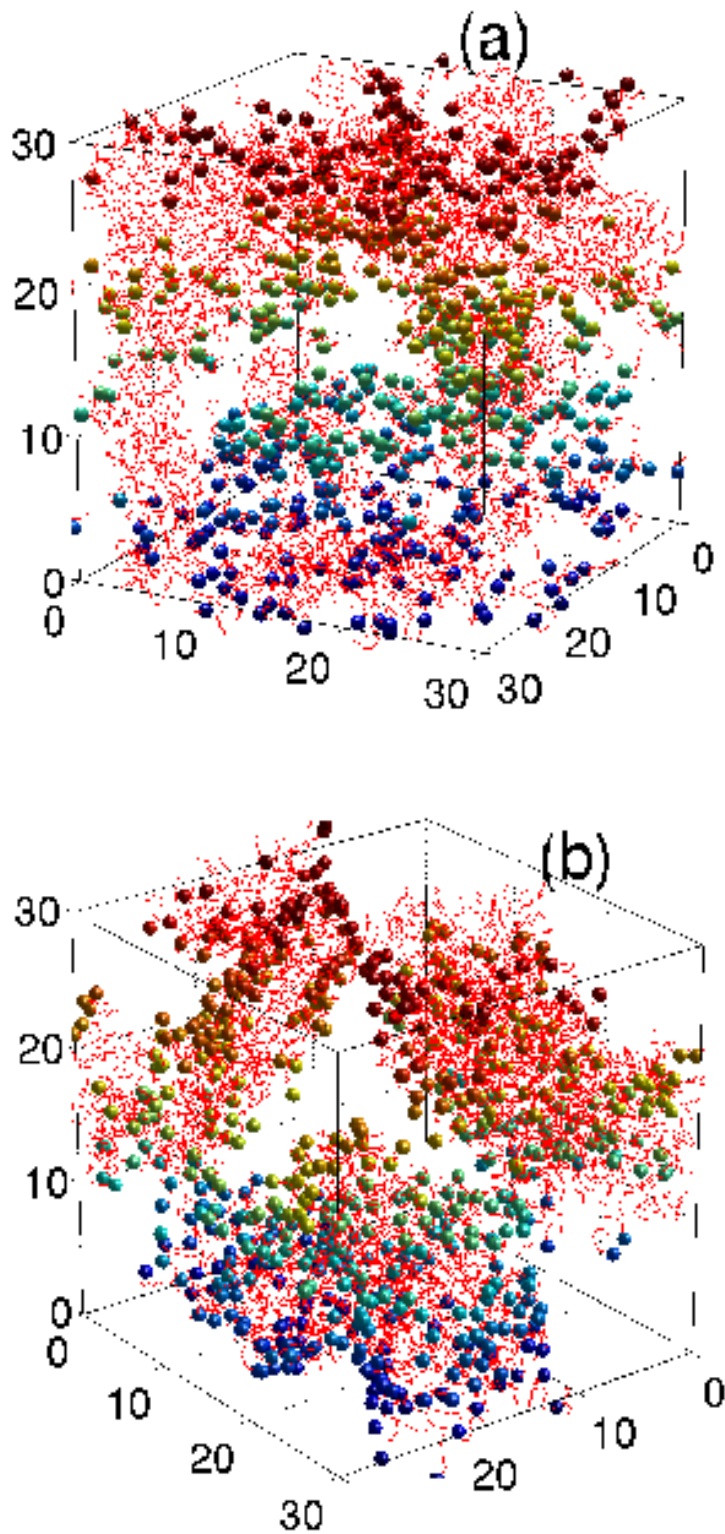


Figure 14: (Color online) Proton-proton structure factor $S(q)$ for Run 8. Dipole strength D_r is scaled down from 1 to 0.

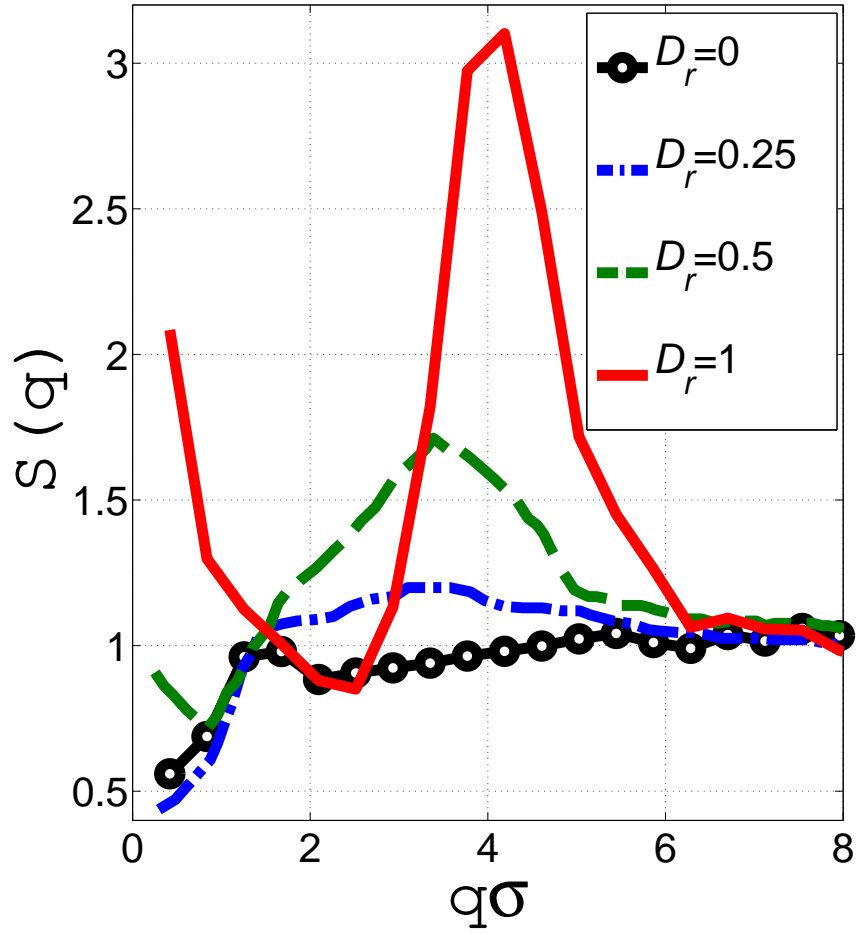


Figure 15: (Color online) Proton-proton pair distribution function $g(r)$ for Runs 7-9 and $Z = 0.1$ (a) and $Z = 0.5$ (b). Z is a fictitious charge on the head groups which causes an artificial Yukawa like attraction between sulfonates. Thick (thin) lines are for $D_r = 0$ ($D_r = 0.5$). Note that the scales on y -axis for short-range and long-range behavior of $g(r)$ (shown as an inset) are different. For other details see the text.

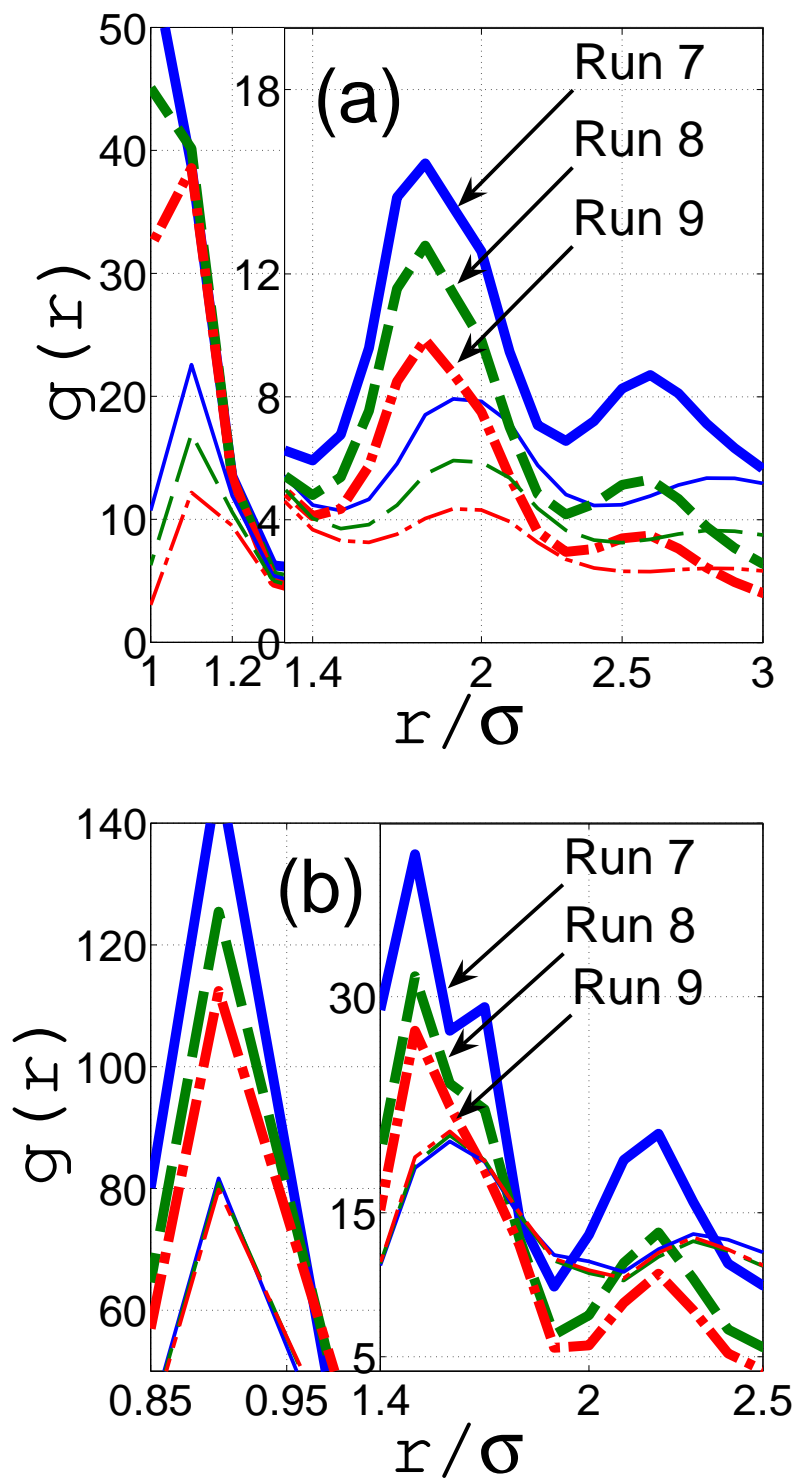


Figure 16: (Color online) Snapshot pictures of systems for Run 9, $n_b\psi = 2$, $D_r=0$, $Z=0.1$ (case (a)) and $Z=0.5$ (case (b)).

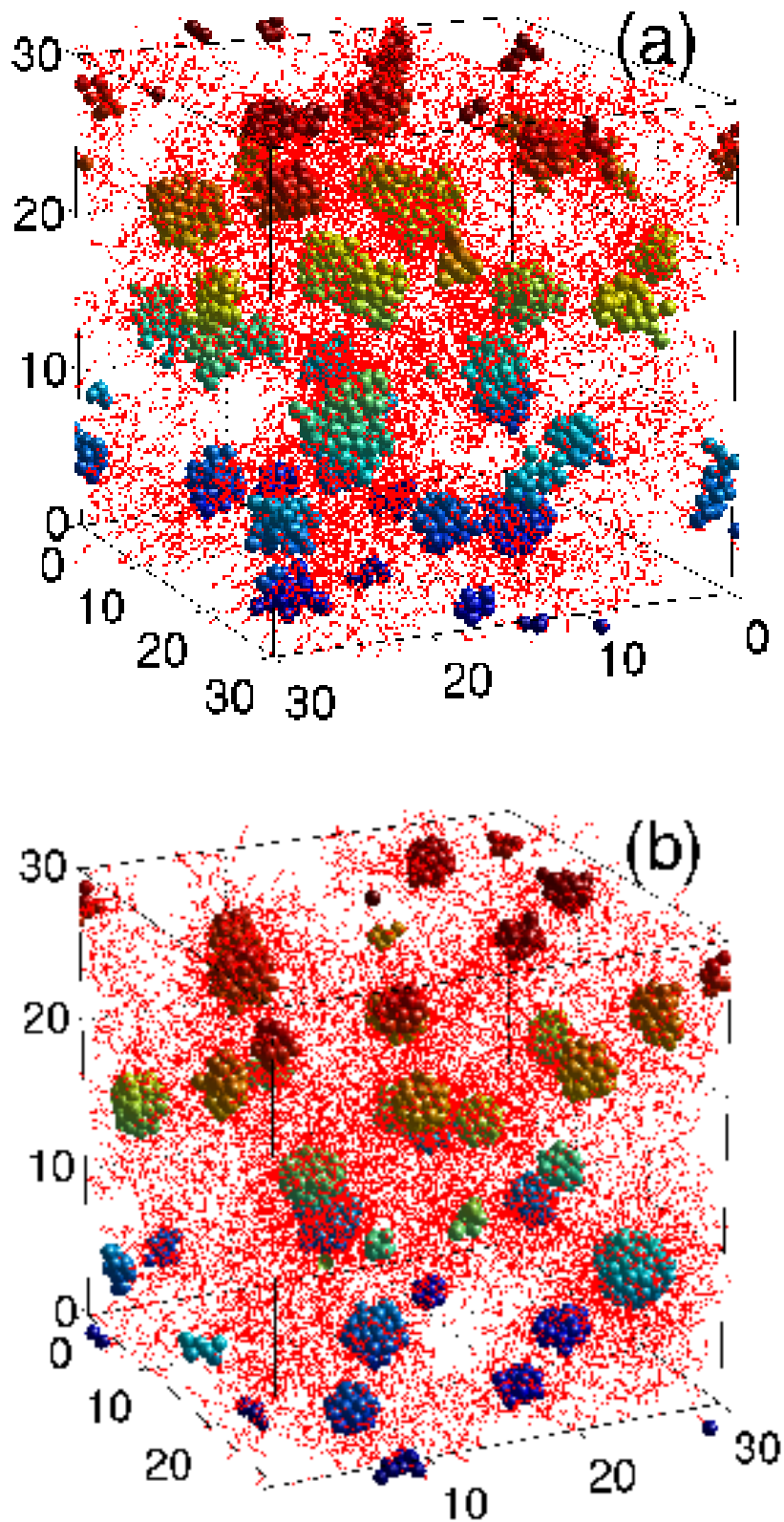


Figure 17: (Color online) Snapshot pictures of systems for Run 9, $n_b\psi = 2$, $D_r=0.5$, $Z=0.1$ (case (a)) and $Z=0.5$ (case (b)).

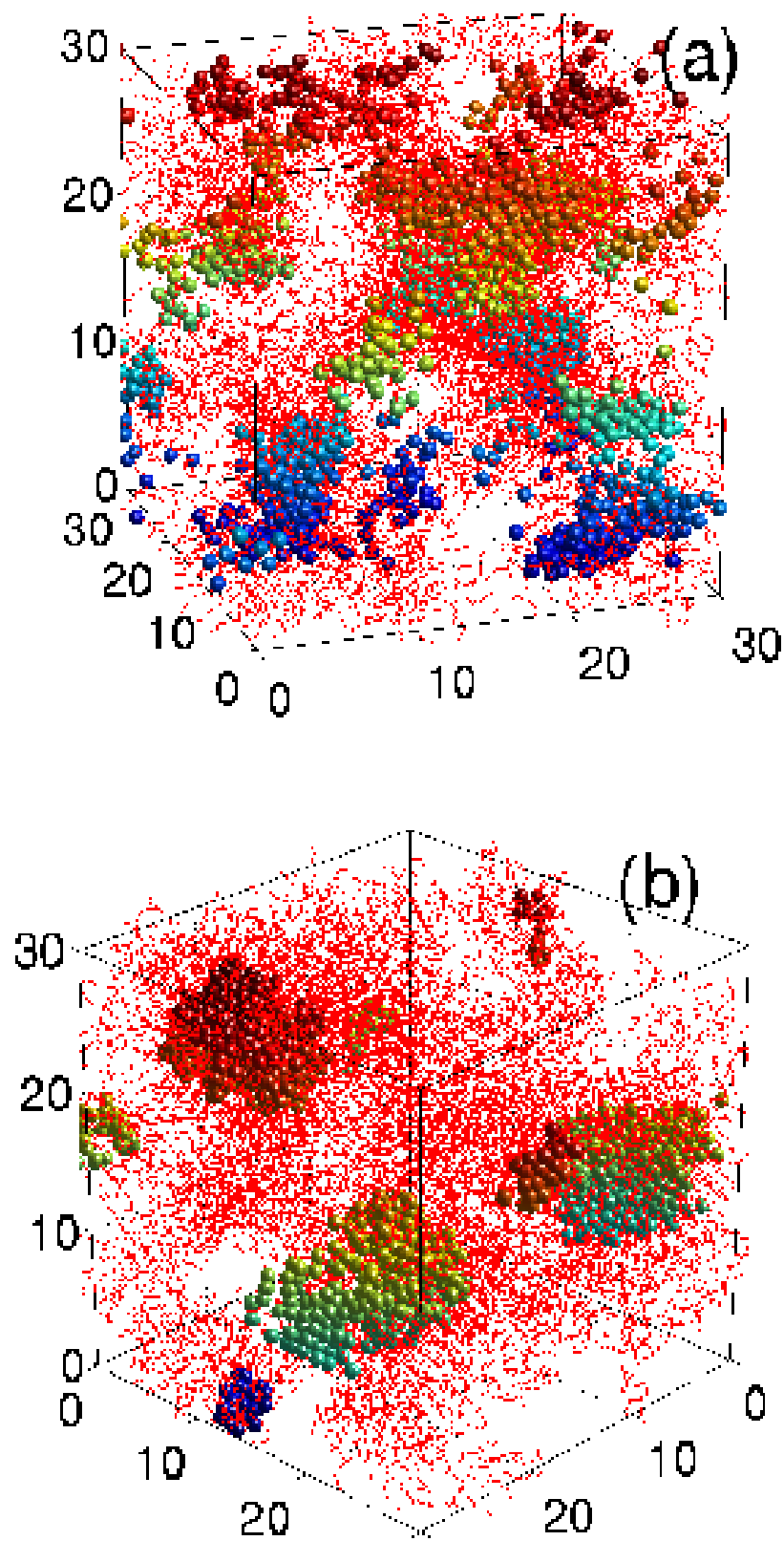


Figure 18: (Color online) Snapshot of a system for Run 9, $n_b\psi = 2$, $D=0.5$, $Z=0$.

